The platelet interior revisited: electron tomography reveals tubular α-granule subtypes

Hezder van Nispen tot Pannerden,[1,2] Felix de Haas,[3] Willie Geerts,[2,4] George Posthuma,[1,2] Suzanne van Dijk,[2,5] and Harry F. G. Heijnen[2,5]

[1]Cell Microscopy Center and Department of Cell Biology, University Medical Center Utrecht, Utrecht; [2]Institute of Biomembranes, Utrecht; [3]FEI Company, Achtseweg, Eindhoven; [4]Molecular Cell Biology, Utrecht University, Utrecht; and [5]Department of Clinical Chemistry and Hematology, University Medical Center Utrecht, Utrecht, The Netherlands

We have used (cryo) electron tomography to provide a 3-dimensional (3D) map of the intracellular membrane organization of human platelets at high spatial resolution. Our study shows that the open canalicular system and dense tubular system are highly intertwined and form close associations in specialized membrane regions. 3D reconstructions of individual α-granules revealed large heterogeneity in their membrane organization. On the basis of their divergent morphology, we categorized α-granules into the following subtypes: spherical granules with electron-dense and electron-lucent zone containing 12-nm von Willebrand factor tubules, subtypes containing a multitude of luminal vesicles, 50-nm-wide tubular organelles, and a population with 18.4-nm crystalline cross-striations. Low-dose (cryo) electron tomography and 3D reconstruction of whole vitrified platelets confirmed the existence of long tubular granules with a remarkably curved architecture. Immuno-electron microscopy confirmed that these extended structures represent α-granule subtypes. Tubular α-granules represent ap-proximately 16% of the total α-granule population and are detected in approximately half of the platelet population. They express membrane-bound proteins GLUT3 and αIIb-β3 integrin and contain abundant fibrinogen and albumin but low levels of β-thromboglobulin and no von Willebrand factor. Our 3D study demonstrates that, besides the existence of morphologically different α-granule subtypes, high spatial segregation of cargo exists within individual α-granules. (*Blood*. 2010;116(7):1147-1156)

Introduction

Blood platelets are the smallest cells in our circulation. They play a central role in the arrest of bleeding after damage of a blood vessel and are crucial elements in the development of thrombosis.[1,2] On injury, platelets rapidly adhere to components of the subendothelium, followed by shape change and subsequent granule secretion.[3] These rapid membrane dynamics are crucial for the progression of platelet-substrate interaction (spreading) and subsequent platelet-platelet interaction (aggregation), ultimately leading to the formation of a platelet plug and the arrest of bleeding.[4] Platelets contain several distinct membrane systems: (1) the open canalicular system (OCS), which is continuous with the cell surface and serves as a membrane reservoir during shape change and spreading[5,6]; (2) the dense tubular system (DTS), representing the platelet smooth endoplasmic reticulum[7]; and (3) secretory organelles. Four types of secretory organelles have been identified in platelets, based on their ultrastructure and selective protein composition: α-granules, dense granules, multivesicular bodies, and lysosomes.[8-10] α-Granules are the major secretory organelles and appear in electron microscopy cross sections as 200- to 500-nm spherical organelles. Platelet α-granules and dense granules are differentially released and play crucial roles in the secondary platelet response.[11,12] Recent studies have suggested the existence of α-granule subclasses with different cargo content and have proposed that these are differentially secreted.[13,14] Conventional transmission electron microscopy (TEM) studies have contributed much to our present understanding of the platelet ultrastructure.[15-18] TEM provides information on the intra-cellular organization of organelles, which, combined with immunogold labeling, enables the visualization of intracellular distribution patterns of molecules with nanometer precision.[19,20] However, TEM provides only 2-dimensional images and is not informative of the membrane continuities in 3 dimensions. Electron microscopy (EM) tomography followed by reconstruction and modeling of the cell provides a way to study the 3-dimensional (3D) organization of membranes and macromolecular structures at nanometer resolution. However, an accurate 3D representation is only achieved when cells are arrested in a close to native state. Vitrification in liquid ethane followed by visualization at cryogene temperature, or high-pressure freezing and low temperature freeze substitution (HPF-FS) immobilize cellular structures in milliseconds.[21] Both methods provide "snapshots" of the cell under near-native physi-ologic conditions. Electron tomography (ET) and reconstruction of the images then allow the snap-frozen structures to be reassembled into a 3D model. In the present study, we have used a combination of ET and immunoelectron microscopy (IEM), as well as HPF-FS technology and visualization of vitrified whole platelets at cryo-genic temperature. Our ET study reveals novel details on the spatial organization of the OCS and DTS. The OCS consists of small neck regions and multiple areas of membrane branching that serve to connect the platelet cell surface from one side to the other at multiple sites. The DTS appears as a reticular membrane system, closely intertwined with the OCS. Our 3D analysis also revealed that the α-granule population is morphologically heterogeneous.

Besides spherical granules and multivesicular subclasses, a tubular granule population also exists. When visualized in whole vitrified platelet samples, these granules appear as long, highly curved membrane strands, connected to spherical domains. IEM analysis and serial cryosectioning confirmed that these tubules represent α-granules. Characterization of the molecular architecture of these granules revealed that high spatial protein segregation exists within individual α-granules. Based on the tubular nature of this α-granule subpopulation and the heterogeneous and spatial protein packaging, we propose that cargo is differentially released from tubular granules compared with spherical granules. Here, we discuss these observations in the context of the developing view on different α-granule populations and their secretion.

Methods

Antibodies and immune reagents

The following antibodies were purchased: AK-6 monoclonal antibody directed to P-selectin was from Serotec. Rabbit polyclonal GPIIb-IIIa antibody was a gift from Dr M. C. Berndt (Melbourne, Australia) and has been previously described.[8] Monoclonal antibody 4A7 directed to β3 integrin chain was from our own department (Hematology, University Medical Center Utrecht). Rabbit polyclonal human fibrinogen and human von Willebrand factor (VWF) antibodies and rabbit anti–mouse IgG were purchased from Dakopatts. Rabbit polyclonal β-thromboglobulin (β-TG) antiserum and GLUT3 antibodies have been described in previous studies.[8,20,22] Anti–human albumin was from Nordic. Monoclonal anti–clathrin heavy chain was from BD Biosciences. The 10-nm and 15-nm protein A gold conjugates were prepared at the Cell Microscopy Center (University Medical Center Utrecht) following standard procedures.

Blood collection and platelet preparation

Whole blood was obtained from normal healthy persons after informed consent was given in accordance with the Declaration of Helsinki. The study was approved by the Medical Ethical Testing Committee of the University Medical Center Utrecht. To avoid preactivation, blood was collected immediately from the vein into fixative (2% glutaraldehyde and 2% paraformaldehyde in 0.1M cacodylate buffer). The fixed platelets were isolated and embedded in Epon according to standard EM procedures. For immunoelectron microscopy, whole blood was collected in a mixture of 2% paraformaldehyde and 0.2% glutaraldehyde in 0.1M phosphate buffer (final concentration). For direct cryoimmobilization (HPF-FS, vitrification), whole blood was collected in 0.34% sodium citrate, and platelet-rich plasma (PRP) was prepared by sedimentation at 180g.

Immunoelectron microscopy

Immunogold labeling of ultrathin cryosections was performed at room temperature by floating the grids on drops containing the diluted antibodies. Immunogold double-labeling was performed using 10-nm and 15-nm protein A gold conjugates (Cell Microscopy Center Utrecht). The sections were evaluated in a JEOL 1200CX electron microscope. For analysis of the VWF and fibrinogen label distribution over tubular and spherical granules, 1000 randomly selected α-granule profiles were scored on thin frozen sections from directly fixed platelets. The relative distribution of other α-granule markers was determined on electron micrographs taken at a nominal magnification of 30 000. Gold particles were counted over tubular and spherical profiles, and their relative surface area was determined from the electron micrographs using a point-hit method. Average label densities over tubules and spherical profiles were calculated by dividing the respective percentages of gold particles by the percentages of line intersections occupied by the structure.

High-pressure freezing and freeze substitution

High-pressure freezing and freeze substitution were performed essentially as described before.[21] In brief, 10 ng/mL PGI2 was added to the PRP, and platelets were carefully sedimented at 300g and resuspended in a small volume of N-2-hydroxyethylpiperazine-N′-2-ethanesulfonic acid Tyrode (0.145mM NaCl, 5mM KCl, 0.5mM Na$_2$HPO$_4$, 1mM MgSO$_4$, 10mM N-2-hydroxyethylpiperazine-N′-2-ethanesulfonic acid, and 5mM D-glucose, pH 7.2) containing 5% bovine serum albumin; 3-μL aliquots of the platelet suspension were pipetted onto golden bovine serum albumin presoaked transfer cups and immediately transferred to a Leica HPF high-pressure freezer (Leica Microsystems) for cryo-immobilization. The samples were stored in liquid nitrogen (LN$_2$) and transferred to the freeze substitution apparatus (Leica AFS, Leica Microsystems), containing pre-cooled substitution fluid of anhydrous acetone, and fixed with 0.5% osmium tetroxide and 0.25% glutaraldehyde in anhydrous acetone at a temperature of −90°C for 48 hours. The temperature was increased by 1°C per hour to −30°C, and this temperature was maintained for 8 hours. The substitution media was washed away by anhydrous acetone, and the cells and grids were embedded in Epon.

Tomography and data analysis

Plastic-embedded sections of 200- to 400-nm thickness were collected and poststained with uranyl acetate and lead citrate. Fiducial markers (10-nm gold particles) were applied to both sides of the section. Where indicated, thick cryosections were collected and embedded in methylcellulose after immunogold labeling. Platelets displaying typical discoid morphologies were selected. Dual-axis tilt series of the cells of interest were then recorded using a Tecnai 20 transmission electron microscope (FEI Company) equipped with a slow scan CCD camera (Temcam F214, TVIPS). After the first tilt series, the specimens were manually rotated over an angle of 90 degrees, and the second tilt series were acquired. Images were recorded automatically with Xplore3D software Version 3.0 (FEI Company) with an angular range from −60 degrees to +60 degrees with 1-degree increment (Tietz CCD camera, 2048 × 2048 pixels, binning 2). The tilt series were aligned using ETOMO Version 3.13.6, a program from the IMOD program package (http://bio3d.colorado.edu), using the fiducial markers and subsequently combined into a 3D volume. The aligned dual-axis tomograms were computed by resolution-weighted back projection. Serial sections were joined together using ETOMO-Join. Within the IMOD program, membrane-bound organelles and structures of interest were manually traced to form a 3D representation of the structure and/or compartment. Membrane-bound organelles were identified using morphologic criteria and immunogold labeling of cryosections.

Low-dose CET

For (cryo) electron tomography (CET), 3-μL aliquots of PRP were pipetted onto glow-discharged Quantifoil 2/2 grids at room temperature in the environmental chamber of a Vitrobot (Mark IV, FEI Company) set at a relative humidity of 100%. Excess fluid was blotted away and the samples were immediately plunge-frozen into liquid ethane. Platelets were also allowed to settle on fibrinogen-coated (100-200 slot grid mesh golden, nickel, copper EM grids, Stork-Veco) for 15 minutes before cryoimmobilization. The grids were stored in LN$_2$. Grids were transferred to a 626 GATAN cryoholder (Gatan) and examined in a FEI Tecnai 12 or 20 (BioTwin) electron microscope. Single-axis tilt series ranging from +65 degrees until −65 degrees with 1-degree increments were collected at −5 μm defocus in low-dose mode. Images were recorded with a 2000 × 2000 pixel FEI Eagle CCD camera. Tomograms were aligned using 10-nm fiducial gold markers and Inspect3D (FEI Company).

Results

For optimal preservation of the steady-state membrane organization, whole blood was collected directly from the vein into fixative.

Figure 1. EM tomography of the intracellular membrane organization in nonstimulated platelet. (A-C) Tomographic slices of directly fixed platelet. Dual axis tilt series were generated from chemically fixed platelets as described in "Tomography and data analysis." The membranes and other structures of interest were manually traced to generate a 3D representation of the structure. Dark blue represents OCS; light blue, platelet secretory α-granule; and red, dense granule. (D) Microtubules are located at the platelet periphery. The OCS membranes are continuous with the cell surface at multiple sites (panel E and arrowheads in panel I), and span the platelet cell surface from one side to the other, revealing numerous branching areas. (An animated model of the OCS is included as supplemental Video 1.) (F-H) Manual tracking of the peripheral microtubular coil (yellow dots at the cell periphery) reveal a microtubule ending at an OCS invagination (supplemental Video 2). α indicates α-granule; δ, dense granule; mt, microtubules; and dts, dense tubular system. (A) Bars represent 200 nm. (B-G) Bars represent 100 nm.
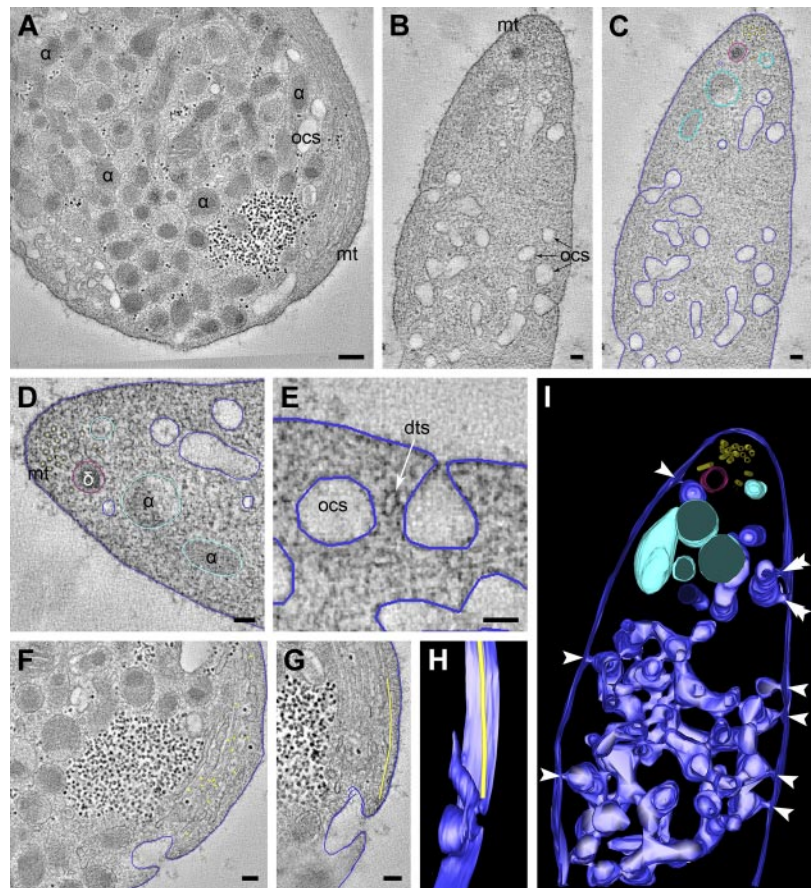
This method provides an elegant way to prevent platelet preactivation during handling. Platelets were also frozen directly in PRP using high-pressure freezing followed by low temperature substitution in fixative (HPF-FS), or vitrified in liquid ethane for immediate visualization at −180°C. The dimensions of the platelet allow whole-cell vitrification in liquid ethane with the vitrobot and subsequent CET. Large volumes can be adequately handled with HPF-FS technology, which provides excellent membrane ultrastructure but has the disadvantage that it requires platelet isolation before cryo-immobilization, which causes preactivation. To determine the spatial membrane organization of the OCS, DTS, and secretory granules in 3D, the use of ET is crucial. Dual-axis tilt series were recorded from 200- to 400-nm-thick plastic sections using both fixation methods, and back-projections were generated to provide 3D reconstructions of the structures of interest. Figure 1 shows an overview of tomographic slices and 3D reconstructions through the resting discoid platelet (supplemental Video 1, available on the *Blood* Web site; see the Supplemental Materials link at the top of the online article).

OCS and DTS are closely intertwined membrane systems

Manual tracking of the cell surface revealed multiple 20- to 30-nm-wide plasma membrane invaginations (Figure 1E, arrowheads in model in Figure 1I), which are continuous with deep intracellular membrane systems representing the OCS. OCS membranes display numerous branching points and span the platelet cell surface from one side to the other, thereby forming a complex reticular membrane network (Figure 1I; supplemental Video 1). Some cell surface OCS openings are closely positioned laterally to the plasma membrane (Figure 1I double arrowheads). Microtu-

bules (MTs) are found in the cell periphery and delineate the plasma membrane in a coiled fashion (Figure 1A,D; supplemental Video 2). Three-dimensional reconstructions of individually traced microtubules showed that some circumferential microtubules end at OCS invaginations (Figure 1F-H). MTs are sometimes incomplete and occasionally reveal physical interconnections (data not shown). The intracellular part of the OCS consists of irregularly shaped vacuolar structures, with frequent tubular neck regions (Figure 2A-B blue arrowheads). The DTS appears as small tubular structures (Figure 2A-B white arrowheads) and is often situated at the cell periphery. Three-dimensional analysis of approximately 300-nm-thick platelet volumes revealed that DTS membranes are in close apposition to OCS structures. They particularly intertwine at the small neck regions that connect individual OCS vacuoles, thereby forming a reticular membrane network (Figure 2; supplemental Video 3). DTS membranes are smooth and do not exhibit signs of ribosomal features. Despite their close positioning to the OCS, no membrane continuities were encountered between the 2 membrane systems.

Identification of α-granule subtypes

α-Granules are the major storage compartments in platelets. Our tomography analysis showed that these membrane-bound organelles display high variability in morphology, size, and luminal content. Three-dimensional reconstruction analyses of individual α-granules are shown in Figures 3 and 4. Tomographic x-y slices, a z-axis orientation, and a reconstructed model are shown in Figure 3A and supplemental Video 4. These data reveal the typical molecular organization of multimeric VWF assemblies. VWF tubules are eccentrically located in the granule body, have an inner
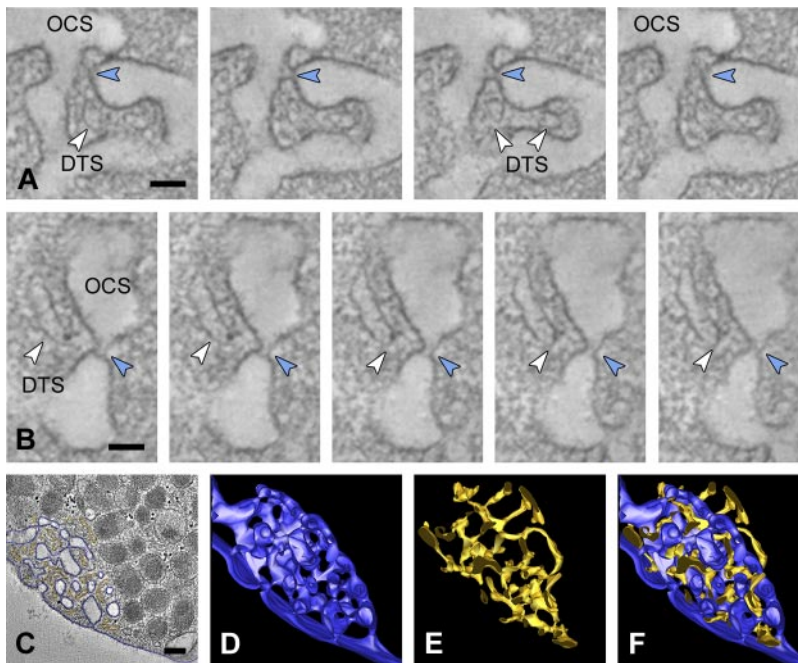
Figure 2. The DTS and OCS are highly intertwined membrane complexes. Dual axis tilt series were generated from chemically fixed platelets as described in "Tomography and data analysis." (A-B) Series of tomographic slices through the OCS membrane complex. Small membrane continuities (blue arrowheads) connect individual OCS vacuoles and are continuous with the cell surface. DTS membranes (white arrowheads) are closely positioned to the OCS neck regions. (C) OCS and DTS membranes were manually traced to generate a 3D representation of the membrane complexes. (D-E) Three-dimensional reconstructions of the OCS (dark blue) and DTS (yellow). (F) Reconstructed model showing the highly intertwined nature of the membrane complexes. (An animated model of the OCS and DTS is included as supplemental Video 3.) (A-B) Bars represent 50 nm. (C) Bars represent 200 nm.

diameter of 11.8 plus or minus 0.4 nm, and are detected only in a subset of the α-granule population. Figure 3B shows a series of tomographic slices extracted from HPF-FS samples. Transverse orientations of the VWF tubules reveal kinked forms (arrows in panel Biii) and helical substructure (highlighted in panel Bv). Besides the characteristic 200- to 500-nm-wide spherical organelles with electron-dense core and electron-lucent areas, we frequently found multivesicular α-granules. In classic 50-nm cryosections sections, but also in HPF-FS samples, these luminal membranes are often obscured by electron-dense matrix proteins (supplemental Figure 1A-B). The model in Figure 3C shows different views of an α-granule immunolabeled with CD63 (red dots) and P-selectin (yellow dot), illustrating that the luminal vesicles are not connected to the limiting membrane. These results demonstrate that the α-granule is a highly compartmentalized organelle, consisting of segregated cargo and separate inner and outer membrane domains.

We frequently encountered organelles with an elongated tubular shape (Figure 4; supplemental Video 5), which became especially apparent after transverse orientation within the tomogram. These elongated structures exhibit a uniform diameter ranging from 40 to 60 nm and are often connected to spherical granules (Figure 4A-C). The tubules are never completely captured in our tomograms (Figure 4D), suggesting an extended "tail" morphology. When properly oriented along their long axis, "tube-like" proteinaceous structures are visible (Figure 4B arrowhead).

Our tomograms often revealed multiple clathrin-coated areas on individual α-granules (supplemental Figure 1). Clathrin-coated lattices are detected on both tubular and spherical organelles. Figure 4E and F show examples of tubular subpopulations connected to spherical domains in sections from HPF-FS samples. Platelets in HPF-FS samples show more signs of activation (ie, filopodial extensions and loss of the peripherally located MT coils). The organelle membranes in such preparations are subjected to less distortion and appear much smoother, revealing the individual granules to be more rounded. The average diameter of the cross-sectioned tubules in HPF-FS samples was in the same range
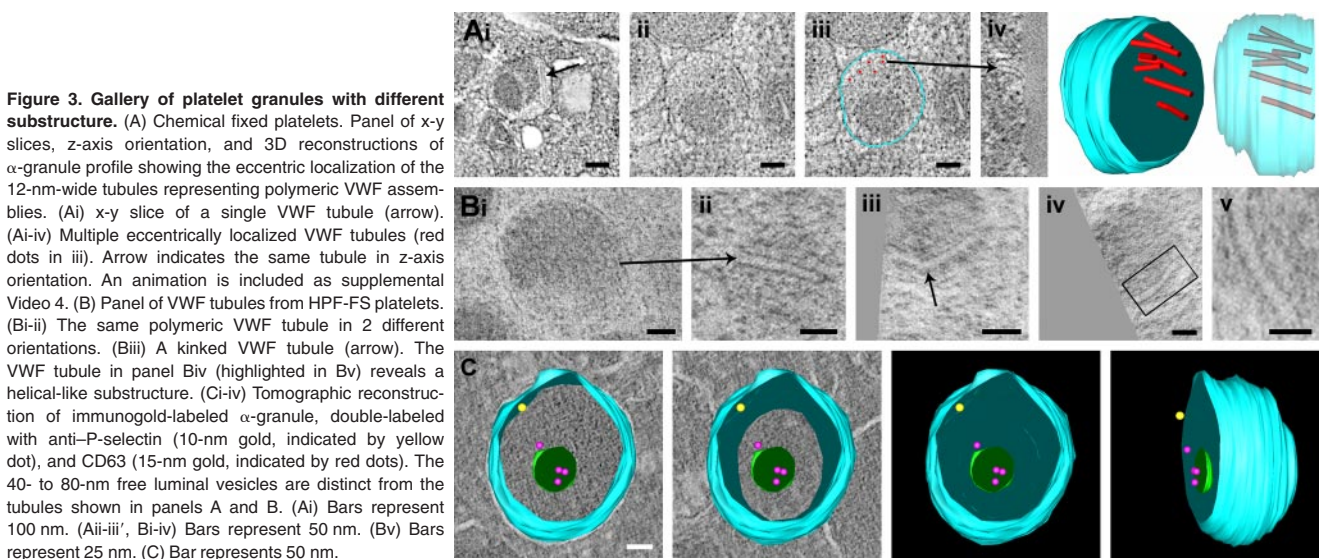

Figure 3. Gallery of platelet granules with different substructure. (A) Chemical fixed platelets. Panel of x-y slices, z-axis orientation, and 3D reconstructions of α-granule profile showing the eccentric localization of the 12-nm-wide tubules representing polymeric VWF assemblies. (Ai) x-y slice of a single VWF tubule (arrow). (Ai-iv) Multiple eccentrically localized VWF tubules (red dots in iii). Arrow indicates the same tubule in z-axis orientation. An animation is included as supplemental Video 4. (B) Panel of VWF tubules from HPF-FS platelets. (Bi-ii) The same polymeric VWF tubule in 2 different orientations. (Biii) A kinked VWF tubule (arrow). The VWF tubule in panel Biv (highlighted in Bv) reveals a helical-like substructure. (Ci-iv) Tomographic reconstruction of immunogold-labeled α-granule, double-labeled with anti–P-selectin (10-nm gold, indicated by yellow dot), and CD63 (15-nm gold, indicated by red dots). The 40- to 80-nm free luminal vesicles are distinct from the tubules shown in panels A and B. (Ai) Bars represent 100 nm. (Aii-iii′, Bi-iv) Bars represent 50 nm. (Bv) Bars represent 25 nm. (C) Bar represents 50 nm.

Figure 4. Series of tomographic slices and 3D models of tubular granule subtypes. (A) Tomographic slice extracted from a semithin cryosection and reconstructed model showing spherical α-granule with developing extension. (B-C) z-axis orientations through tubular α-granule subtypes obtained from chemical fixed resting platelets. For details, see "Tomography and data analysis." (B) Fibrillar protein densities (arrows) are apparent within the tubule. (C) Tubular profile connected to a spherical domain. (An animated model is included as supplemental Video 5.) (D) Tomographic slice and 3D model of multiple tubules (light blue) extracted from an approximately 300-nm section of a chemical fixed platelet. (E-F) Tubular and spherical granules extracted from HPF-FS platelets. (E) Several cross-sectioned tubules are shown (arrowheads). (F) Tubule (arrowhead) connected to a spherical granule (☆). White arrowheads indicate (obscured) luminal membranes within α-granule subtypes. Bars represent 100 nm.
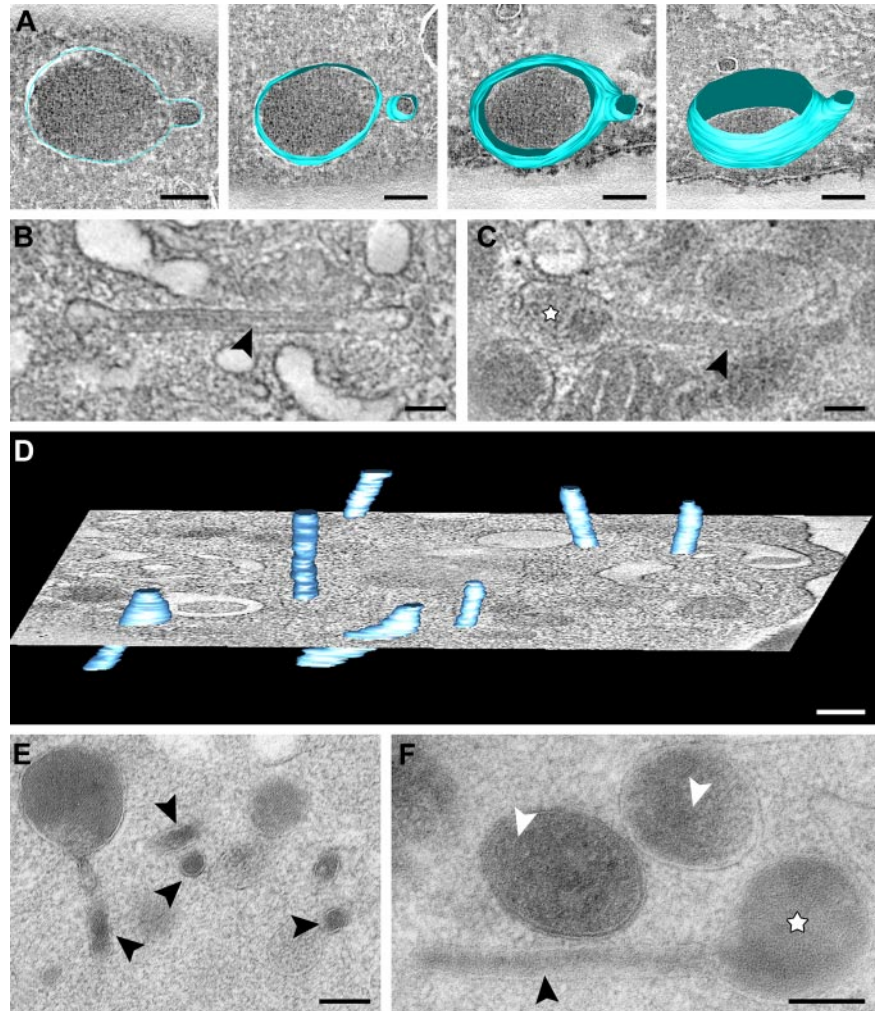
(49.6 ± 5.5 nm; n = 26) as measured from chemically fixed samples (49.7 ± 6.5 nm; n = 29).

CET of whole vitrified platelets reveals spherical granules and tubules

To obtain insight into the spatial organization of α-granules within the whole cell, we took advantage of the small size of the platelet and performed CET. PRP was frozen in liquid ethane after EM analysis at −180°C. Snapshots taken from cryoimmobilized preparations reveal a great variety in the morphology of α-granules (Figure 5). Vitrified spherical granules exhibit highly smoothened limiting membranes with variable electron-dense content and the presence of luminal membranes (Figure 5A). α-Granules with extended tail morphology were frequently detected in whole vitrified platelets (Figure 5B). This subpopulation of α-granules is observed as long tubular strands (Figure 5B arrowheads) and exhibits typical electron-dense spherical domains at one extreme end (Figure 5B white star). To obtain a 3D image within the whole vitrified cell, single-axis tilt series were generated at low-dose mode and data were reconstructed into a 3D model after denoising and manual surface rendering. Figure 5C through F shows 4 tomographic slices with different orientations of the tubular organelle. Total length of the structure is 7.6 μm, and its spherical domain measures 220 nm. The tubule thickness ranges from 31 nm to 65 nm. A 3D reconstruction is shown in Figure 5G and H and supplemental Video 6.

The elongated membrane strands represent α-granule subtypes

To further characterize the long tubular granule subpopulation, we next analyzed ultrathin cryosections after immunogold labeling with established α-granule markers. Because of limited Z-resolution of thin cryosections, tubular profiles are less frequently detected with their long axis oriented in the plane of the section. As a result, they appear in cross sections mostly as 40- to 60-nm-wide spherical profiles (Figure 4). With this notion in mind, we counted the number of platelets exhibiting tubular profiles and found that just more than 40% of the cells contain one or more tubular profiles (n = 500 cells). When we classified the granule subtypes into tubular (40-60 nm diameter) and spherical morphologies (> 200 nm), we found that spherical subtypes predominate (84% spherical vs 16% tubular granules, n = 500 cells). Consistent with our observations in vitrified platelets, in cryosections we also found that tubules were physically connected to spherical granules. A selection of tubular granule profiles from immunolabeled ultrathin cryosections is shown in Figures 6 and 7. Membrane-bound α-granule proteins αIIb-β3 integrin and GLUT3 can be readily detected on the tubules identifying them as α-granules, whereas trace P-selectin was observed (Figure 6). A subset of the tubular-shaped α-granules showed a distinct cross-striation pattern with a periodicity of 18.5 plus or minus 0.4 nm, reminiscent of fibrin polymers (supplemental Figure 2). In the cross-striated areas, fibrinogen was abundant present but not VWF.
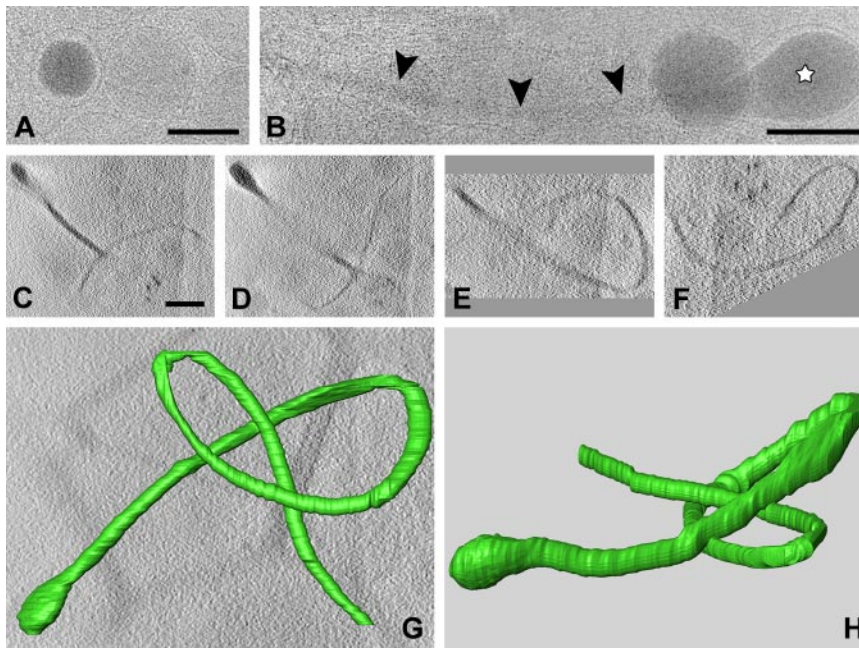
Figure 5. CET of whole vitrified platelet. (A-B) Snapshots extracted from a whole vitrified platelet in PRP, plunge frozen in liquid ethane. Spherical and extended granule subtypes are shown. (A) Note the difference in electron density of individual spherical granules. Luminal vesicles are visible in the granule on the righthand side of panel A. (B) Tubular profiles (arrowheads) are often connected to electron-dense spherical domains (☆). (C-F) Tomographic slices of a tubular granule subtype extracted from a vitrified platelet after single-axis tilting and low-dose recording at −5 μm defocus. The tubular strand is more than 7 μm long and exhibits a highly curved nature. (G) Reconstructed 3D model (top view) after manual surface rendering with IMOD software. (H) Side view (an animation is included as supplemental Video 6). Bars represent 100 nm.

VWF is absent from tubular profiles

Because α-granule cargo is derived from both biosynthetic and endocytic origin, we next asked whether differences exist in the cargo distribution between tubular and spherical granules. A quantitative evaluation of the gold-labeling patterns showed that VWF and β-TG were almost exclusively localized in the spherical granules and undetectable in tubular granules, whereas fibrinogen was equally distributed over both subpopulations (Figure 6). Albumin was also abundantly detected in both subtypes but was present in the tubules to a lesser extent. Furthermore, within the subset of spherical granules, 41.8% plus or minus 7.5% showed colocalization of VWF and fibrinogen, whereas 45.5% plus or minus 7.2% contained exclusively fibrinogen, and 12.8% plus or minus 3.9% only VWF (Figure 6G; n = 1000 α-granules). Thus, VWF and β-TG are selectively excluded from tubular α-granules. To obtain detailed information on the spatial protein segregation, we next combined serial cryosectioning with immunogold labeling. Using this approach, we found that connections exist between fibrinogen-positive tubules and VWF-positive spherical granules (supplemental Figure 3). Furthermore, subsequent cross sections of the same granule exposed different subpopulations (ie, dense core or multivesicular granules; supplemental Figure 1A-B). Together, these observations demonstrate that, besides different morphologies, high spatial protein segregation also exists within individual α-granule subtypes.

Discussion

In the present study, we provide "snapshots" of the steady-state membrane organization of the resting blood platelet, under conditions close to their physiologic state. We analyzed the spatial organization of 2 crucial membrane complexes, the OCS and the DTS, using ET. Our findings confirm previous reports, defining the OCS as a reticular membrane network with numerous branching channels and multiple cell surface connections.[6] Three-dimensional reconstruction analysis shows that vacuolar regions of the OCS are interconnected through small membrane neck regions.

DTS membranes are in close proximity to the small OCS neck regions, but no sign of membrane connections between both membrane systems is observed. The OCS has an important role as a membrane storage compartment. Platelet spreading requires the contribution of intracellularly stored OCS membranes.[23] In a similar fashion, a membrane supply from internal stores is probably required in the formation of long membrane tethers, a key step in the platelet adhesion process under fast-flowing conditions. Tether formation does not require platelet activation and is independent of granule secretion,[24] suggesting that additional membrane must derive from the OCS. To accommodate this shear-dependent outward membrane flow, rapid changes must occur in the membrane geometry of the OCS. Based on the spatial membrane topology of the OCS, we propose that membrane-evaginating processes, such as tether formation and spreading, require the homotypic fusion of OCS membranes. The small neck regions connecting OCS vacuoles may be possible targets for severing by a dynamin-related protein. An important observation from our 3D analysis was the close association and intertwined nature of the reticular DTS with the OCS. Whether critical positioning of the DTS plays a role in regulating OCS fusion remains an intriguing question to be addressed. It is well established that the DTS is the calcium store for cell activation and membrane fusion events. Close proximity of the DTS to extracellular OCS membranes may serve to gain rapid access to the DTS and transfer extracellular signals for local release of calcium.

A major focus of the current study was to define the spatial organization of the secretory α-granule population at high resolution. Using 3D analysis and combined IEM characterization, we have further defined the different classes of α-granules (supplemental Table 1). Based on morphology and substructure, we distinguished: (1) spherical granules exhibiting a heterogeneous matrix substructure with electron-dense and electron-lucent zones, (2) multivesicular subtypes displaying a multitude of free luminal membrane vesicles, and (3) a distinct population of approximately 50-nm-wide tubular granules, which we have designated tubular α-granules. A subset of the spherical granules displayed peripheral approximately 12-nm-wide tubules, representing multimeric forms

Figure 6. IEM characterization of granule subtypes. Platelets were fixed for immunoelectron microscopy as described in "Blood collection and platelet preparation." Immunogold labeling was performed on 50-nm-thick cryosections, and the samples were analyzed on a JEOL 1200CX electron microscope. (A-F) Tubular granules were identified as α-granule after immunogold labeling with specific α-granule markers. Labeling of soluble (A-D) and integral membrane proteins (E-F) as indicated on the figures. (G) Quantification of the immunogold label over tubular and spherical profiles. Label densities were determined on electron micrographs at 30 000× nominal magnification, by dividing the total number of gold particles attributed to each subtype by the number of random intersections over the structure. For each marker, a total of 20 electron micrographs was evaluated. Label density is expressed in arbitrary units. Bars represent 200 nm.
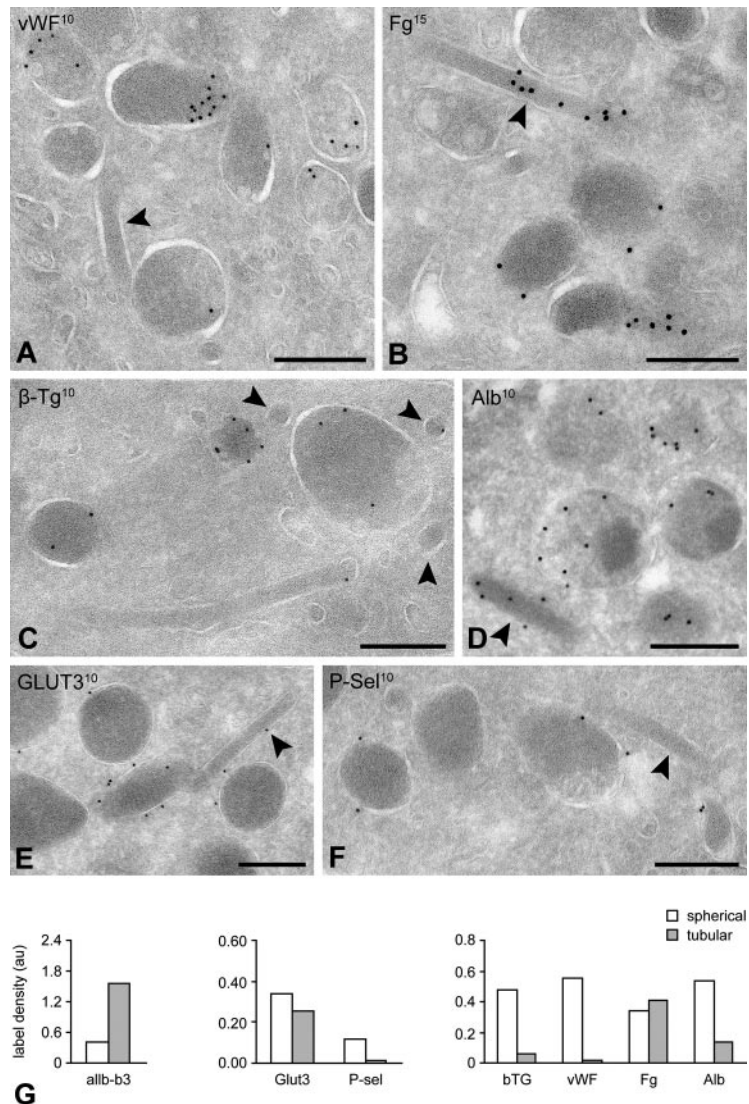
of VWF.[19] Elongated subpopulations of α-granules often exhibit a fibrin-like approximately 18-nm cross-striation pattern. The extended nature of the tubular α-granules was particularly highlighted in CETs of vitrified whole platelets, where they appear as highly curved strands reaching lengths of up to 7 μm. Tubular strands were frequently detected but were not seen in all platelets, an observation reflected by the high proportion of cells (41%) exhibiting the typical cross-sectioned approximately 50-nm-wide profiles. Long filamentous membranous structures have previously been demonstrated in platelet whole mounts and, based on their electron-dense appearance, were considered to be dense granules.[25] Recent EM observations have challenged this conclusion and suggested that these tubular membranes may represent α-granules.[26] Our present study confirms this hypothesis and provides evidence that the tubular strands represent α-granules. EM tomography and IEM revealed that these tubular strands are connected to spherical granules and that cargo proteins are differentially segregated within these α-granule subtypes.

Platelet α-granules share several characteristics with Weibel-Palade bodies in endothelial cells. Both organelles contain tubular VWF assemblies (abundant in Weibel-Palade bodies but present only in a subset of the α-granules) and also express the membrane-bound proteins CD63 and P-selectin.[8,27] There is consensus that the tubular shape of Weibel-Palade bodies is determined by specific packaging of VWF multimers into tubular assemblies.[28] However, in platelets, tubular assemblies, and VWF immunolabeling is restricted to a subset of the spherical granules and absent from tubules. It is therefore unlikely that the elongated shape of this subtype is related to VWF packaging. α-Granules acquire their protein content via 2 distinct pathways, namely, via biosynthetic and endocytic routes.[29,30] Proteomic analysis of α-granules[31] and their released content[32] has demonstrated that α-granules contain cargo proteins with apparent opposite functions, leading to the suggestion that these proteins are stored in distinct α-granules.[13,14] These observations have led to the belief that proteins from endocytic origin are selectively delivered to a subpopulation of α-granules.[33] In agreement with this, we find distinct distribution patterns for endocytic and biosynthetic cargo proteins in morphologically distinct α-granules. From the combined 3D and IEM analysis, it appears that tubules are connected to subsets of the spherical granule population and that high spatial segregation of cargo exists with respect to these structures. These observations raise questions regarding the true existence of α-granule subsets with distinct protein composition. Considering the fact that tubular α-granules represent a minority of total α-granules, there is still a
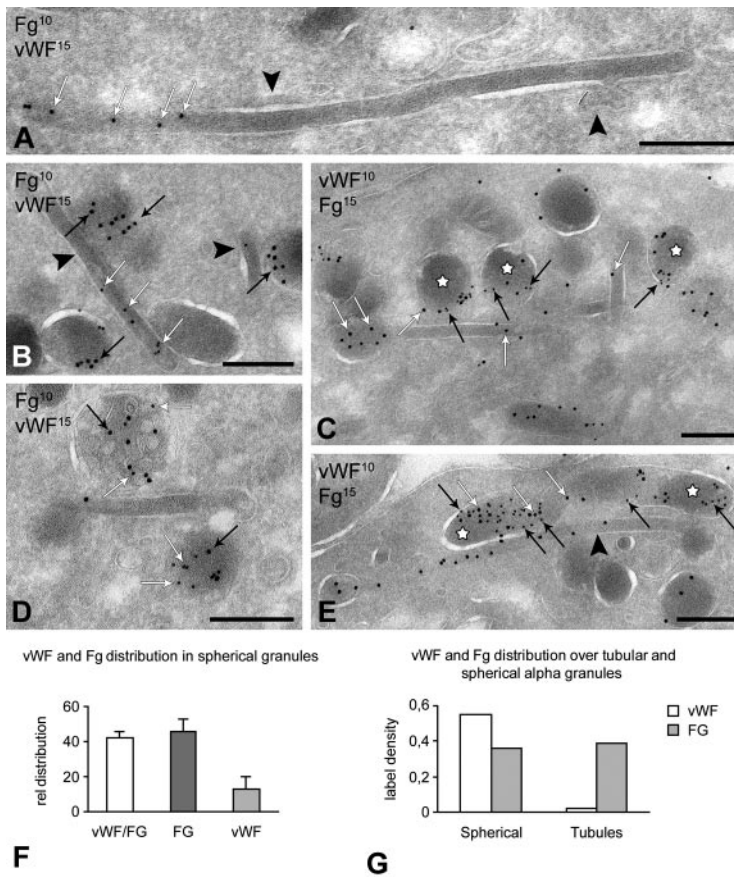
Figure 7. Segregation of VWF from tubular α-granules. Platelets were fixed for immunoelectron microscopy as described in "Blood collection and platelet preparation." Immunogold double-labeling was performed on approximately 60-nm-thick cryosections using 10-nm and 15-nm protein-A gold and analyzed on a JEOL 1200CX electron microscope. (A-E) Immunogold double labeling of VWF and fibrinogen in tubular and spherical granules. Labeling as indicated on the figures. White arrows indicate fibrinogen; and black arrows, VWF. (A) Long tubular profile showing distinct fibrinogen labeling at one end. VWF is absent from the tubules. Clathrin lattices are indicated by the arrowheads. (B-E) Fibrinogen is distributed over both subtypes. VWF and fibrinogen colocalize in spherical (C,E, ☆) and multivesicular subtypes (D). Spheres exclusively containing fibrinogen are also prominent (B,E). Tubular profiles containing fibrinogen but no VWF are indicated by arrowheads in panels B and E. Note that the sequence of immunogold labeling in panels C and E is reversed. (F-G) Quantitative evaluation of the VWF and Fg distribution and colocalization over spherical and tubular subtypes (n = 1000 granules). Bars represent 200 nm.

possibility that an autonomous spherical α-granule population exists with separate protein content.

Our findings also raise important questions with respect to the physiology of granule formation and secretion. Segregation in tubular domains may come from the fusion of separate rod-shaped (possibly of endocytic origin) granules with spherical subtypes (possibly of biosynthetic origin), thereby giving rise to hybrid organelles with partial protein segregation and partial colocalization. Alternatively, the extent to which these structures are covered with clathrin lattices suggests an important role for this coat. Quantitative evaluation of clathrin immunolabeling revealed that clathrin was equally distributed on tubular and spherical α-granules. We found flat and highly curved clathrin lattices on both granule types. The highly curved clathrin lattices probably represent budding profiles of vesicles in their formative stage. Flat clathrin coats on multivesicular endosomes have been postulated to facilitate selective protein sorting toward the luminal vesicles.[21,34,35] Flat clathrin lattices on α-granules may serve a function in generating separate inner and outer membrane domains and simultaneously contribute to the formation of a protein gradient and the compartmentalized nature of these organelles. Abundant presence of clathrin lattices has been observed on Weibel-Palade bodies as well and was suggested to be implicated in the sorting of membrane proteins and in providing a scaffold for organelle structure.[36,37]

The secretory pathway in platelets has been subject to several studies, and it is well established that the OCS serves as an important route for cargo release.[5] Recent studies have suggested that the kinetics of fibrinogen and VWF secretion, and of proangiogenic and antiangiogenic proteins, stems from differential release of α-granule subtypes, a process that may be regulated by different agonists.[33,38] In this context, the comparison of tubular α-granules and Weibel-Palade bodies is remarkable. Two mechanisms have been proposed for the differential secretion of Weibel-Palade body cargo: (1) selective, time-dependent release via the formation of small fusion pores,[39] or (2) differential release as a result of the heterogeneous nature of these organelles.[40] Rab27b is responsible for anchoring and fusion of Weibel-Palade bodies with the plasma membrane, and it is suggested that fusion occurs preferentially with their short ends.[40] Based on the present findings, we propose that the heterogeneous nature of the α-granule population may result in a differential secretory behavior. With this is mind, we think that the kinetics of cargo release from long tubular profiles will be different for spherical granules. Assuming that tubules fuse preferentially via their short ends with OCS or plasma membrane, the spatial protein segregation will probably result in a time-dependent secretion of the protein gradient from this compartment. Platelets contain the Rab GTPases Rab 27a,b,[41,42] and several t-SNARE proteins, including SNAP-23, Syntaxins 2 and 4,[43,44] and the v-SNARES VAMP 3 and 8.[45,46] These SNARE partners are required for the selective fusion of secretory granules with their target membranes.[46-48] Rab27b (H.F.G.H., unpublished observation) and the t-SNARE proteins cellubrevin, SNAP23, and syntaxin-2 have been identified on platelet α-granules.[49] Whether these fusogenic proteins are differentially distributed over α-granule subtypes, presumably giving rise to differential secretory behavior, remains to be determined.[48]

In conclusion, the current study has provided a detailed 3D view of the spatial membrane topology of the OCS, DTS, and secretory α-granule population within the resting human platelet. Particularly striking was the discovery of an extended and highly curved α-granule subtype. Using combined EM tomography and IEM

analysis, we show that high spatial protein gradients exist within this compartment. We propose that tubular α-granules have different secretory capacities compared with classic spherical granules and that spatial segregation of cargo within the tubular subtypes may lead to differential release of their content. Having defined and mapped the ultrastructure of these organelles, it will be important to further characterize their relationship with the kinetics of platelet secretion in functional assays. Finally, our study underscores the importance of high-resolution ET to resolve the spatial organization of complex membrane systems, such as OCS, DTS, and individual platelet organelles. There is a challenge to adapt ET for the analysis of the platelet secretory behavior to better appreciate time-dependent and agonist-selective release phenomena.

Authorship

Contribution: H.v.N.t.P. performed the 3D tomography and drafted the paper; F.d.H. performed the low-dose CET analysis; S.v.D. performed the cryosectioning and IEM analysis; W.G. participated in the acquisition of the 3D data; G.P. performed the quantitative IEM evaluation and participated in revising the manuscript; and H.F.G.H. supervised the study and drafted and wrote the paper.

Conflict-of-interest disclosure: F.d.H. is employed by FEI Company, Achtseweg Eindhoven, The Netherlands. The remaining authors declare no competing financial interests.

Correspondence: Harry F. G. Heijnen, Department of Clinical Chemistry and Hematology, and Cell Microscopy Center, University Medical Center Utrecht, Heidelberglaan 100, 3584 CX Utrecht, The Netherlands; e-mail: h.f.g.heijnen@umcutrecht.nl.

References

1. Michelson AD. *Platelets.* San Diego, CA: Academic Press; 2002.

2. Ruggeri ZM. Platelets in atherothrombosis. *Nat Med.* 2002;8(11):1227-1234.

3. Reed GL, Fitzgerald ML, Polgar J. Molecular mechanisms of platelet exocytosis: insights into the 'secrete' life of thrombocytes. *Blood.* 2000; 96(10):3334-3342.

4. Wester J. The hemostatic plug. *Semin Hematol.* 1977;14(3):265-299.

5. Escolar G, Leistikow E, White JG. The fate of the open canalicular system in surface and suspension-activated platelets. *Blood.* 1989;74(6):1983-1988.

6. White JG, Clawson CC. The surface-connected canalicular system of blood platelets: a fenestrated membrane system. *Am J Pathol.* 1980;101(2): 353-364.

7. van Nispen tot Pannerden HE, van Dijk SM, Du V, Heijnen HFG. Platelet protein disulfide isomerase is localized in the dense tubular system and does not become surface expressed after activation. *Blood.* 2009;114(21):4738-4740.

8. Heijnen HF, Debili N, Vainchencker W, Breton-Gorius J, Geuze HJ, Sixma JJ. Multivesicular bodies are an intermediate stage in the formation of platelet alpha-granules. *Blood.* 1998; 91(7):2313-2325.

9. Sixma JJ, Slot J-W, Geuze HJ. Immunocytochemical localization of platelet granule proteins. *Methods Enzymol.* 1989;169:301-311.

10. White JG. The dense bodies of human platelets: inherent electron opacity of the serotonin storage particles. *Blood.* 1969;33(4):598-606.

11. Lemons PP, Chen D, Whiteheart SW. Molecular mechanisms of platelet exocytosis: requirements for [alpha]-granule release. *Biochem Biophys Res Commun.* 2000;267(3):875-880.

12. Shirakawa R, Higashi T, Tabuchi A, et al. Munc13-4 Is a GTP-Rab27-binding protein regulating dense core granule secretion in platelets. *J Biol Chem.* 2004;279(11):10730-10737.

13. Sehgal S, Storrie B. Evidence that differential packaging of the major platelet granule proteins von Willebrand factor and fibrinogen can support their differential release. *J Thromb Haemost.* 2007;5(10):2009-2016.

14. Italiano JE Jr, Richardson JL, Patel-Hett S, et al. Angiogenesis is regulated by a novel mechanism: pro- and antiangiogenic proteins are organized into separate platelet α granules and differentially released. *Blood.* 2008;111(3):1227-1233.

15. Behnke O. Electron microscopic observations on the membrane systems of the rat blood platelet. *Anat Rec.* 1967;158(2):121-137.

16. Behnke O, Zelander T. Substructure in negatively stained microtubules of mammalian blood platelets. *Exp Cell Res.* 1966;43(1):236-239.

17. Heijnen HF, Schiel AE, Fijnheer R, Geuze HJ, Sixma JJ. Activated platelets release two types of membrane vesicles: microvesicles by surface shedding and exosomes derived from exocytosis of multivesicular bodies and alpha-granules. *Blood.* 1999;94(11):3791-3799.

18. White JG. Use of the electron microscope for diagnosis of platelet disorders. *Semin Thromb Hemost.* 1998;24(2):163-168.

19. Cramer EM, Meyer D, le Menn R, Breton-Gorius J. Eccentric localization of von Willebrand factor in an internal structure of platelet alpha-granule resembling that of Weibel-Palade bodies. *Blood.* 1985;66(3):710-713.

20. Heijnen HF, Oorschot V, Sixma JJ, Slot JW, James DE. Thrombin stimulates glucose transport in human platelets via the translocation of the glucose transporter GLUT-3 from alpha-granules to the cell surface. *J Cell Biol.* 1997;138(2):323-330.

21. Murk JLAN, Humbel BM, Ziese U, et al. Endosomal compartmentalization in three dimensions: implications for membrane fusion. *Proc Natl Acad Sci U S A.* 2003;100(23):13332-13337.

22. Sander HJ, Slot JW, Bouma BN, Bolhuis PA, Pepper DS, Sixma JJ. Immunocytochemical localization of fibrinogen, platelet factor 4, and beta thromboglobulin in thin frozen sections of human blood platelets. *J Clin Invest.* 1983;72(4):1277-1287.

23. Zucker-Franklin D, Benson KA, Myers KM. Absence of a surface-connected canalicular system in bovine platelets. *Blood.* 1985;65(1):241-244.

24. Reininger AJ, Heijnen HFG, Schumann H, Specht HM, Schramm W, Ruggeri ZM. Mechanism of platelet adhesion to von Willebrand factor and microparticle formation under high shear stress. *Blood.* 2006;107(9):3537-3545.

25. White JG. Giant electron-dense chains, clusters and granules in megakaryocytes and platelets with normal dense bodies: an inherited thrombocytopenic disorder. *Platelets.* 2003;14(5):109-121.

26. White JG. Electron opaque structures in human platelets: which are or are not dense bodies? *Platelets.* 2008;19(6):455-466.

27. Harrison-Lavoie KJ, Michaux G, Hewlett L, et al. P-Selectin and CD63 use different mechanisms for delivery to Weibel-Palade bodies. *Traffic.* 2006;7(6):647-662.

28. Huang R-H, Wang Y, Roth R, et al. Assembly of Weibel Palade body-like tubules from N-terminal domains of von Willebrand factor. *Proc Natl Acad Sci U S A.* 2008;105(2):482-487.

29. Handagama P, Rappolee DA, Werb Z, Levin J, Bainton DF. Platelet alpha-granule fibrinogen, albumin, and immunoglobulin G are not synthesized by rat and mouse megakaryocytes. *J Clin Invest.* 1990;86(4):1364-1368.

30. Harrison P, Wilbourn B, Debili N, et al. Uptake of plasma fibrinogen into the alpha granules of human megakaryocytes and platelets. *J Clin Invest.* 1989;84(4):1320-1324.

31. Maynard DM, Heijnen HFG, Horne MK, White JG, Gahl WA. Proteomic analysis of platelet alpha granules using mass spectrometry. *J Thromb Haemost.* 2007;5(9):1945-1955.

32. Coppinger JA, Cagney G, Toomey S, et al. Characterization of the proteins released from activated platelets leads to localization of novel platelet proteins in human atherosclerotic lesions. *Blood.* 2004;103(6):2096-2104.

33. Italiano JE Jr, Battinelli EM. Selective sorting of alpha-granule proteins. *J Thromb Haemost.* 2009;7(1):173-176.

34. Raposo G, Tenza D, Murphy DM, Berson JF, Marks MS. Distinct protein sorting and localization to premelanosomes, melanosomes, and lysosomes in pigmented melanocytic cells. *J Cell Biol.* 2001;152(4):809-824.

35. Sachse M, Urbe S, Oorschot V, Strous GJ, Klumperman J. Bilayered clathrin coats on endosomal vacuoles are involved in protein sorting toward lysosomes. *Mol Biol Cell.* 2002;13(4): 1313-1328.

36. Metcalf DJ, Nightingale TD, Zenner HL, Lui-Roberts WW, Cutler DF. Formation and function of Weibel-Palade bodies. *J Cell Sci.* 2008; 121:19-27.

37. Zenner HL, Collinson LM, Michaux G, Cutler DF. High-pressure freezing provides insights into Weibel-Palade body biogenesis. *J Cell Sci.* 2007; 120:2117-2125.

38. Klement GL, Yip TT, Cassiola F, et al. Platelets actively sequester angiogenesis regulators. *Blood.* 2009;113(12):2835-2842.

39. Babich V, Meli A, Knipe L, et al. Selective release of molecules from Weibel-Palade bodies during a lingering kiss. *Blood.* 2008;111(11):5282-5290.

40. Cleator JH, Zhu WQ, Vaughan DE, Hamm HE. Differential regulation of endothelial exocytosis of P-selectin and von Willebrand factor by protease-activated receptors and cAMP. *Blood.* 2006;107(7):2736-2744.

41. Barral DC, Ramalho JS, Anders R, et al. Functional redundancy of Rab27 proteins and the pathogenesis of Griscelli syndrome. *J Clin Invest.* 2002;110(2):247-257.

42. Tolmachova T, Abrink M, Futter CE, Authi KS, Seabra MC. Rab27b regulates number and secretion of platelet dense granules. *Proc Natl Acad Sci U S A.* 2007;104(14):5872-5877.

43. Chen D, Lemons PP, Schraw T, Whiteheart SW. Molecular mechanisms of platelet exocytosis: role of SNAP-23 and syntaxin 2 and 4 in lysosome release. *Blood.* 2000;96(5):1782-1788.

44. Houng A, Polgár J, Reed GL. Munc18-syntaxin complexes and exocytosis in human platelets. *J Biol Chem.* 2003;278(22):19627-19633.

45. Polgar J, Chung S-H, Reed GL. Vesicle-associated membrane protein 3 (VAMP-3) and VAMP-8 are present in human platelets and are required for granule secretion. *Blood.* 2002;100(3):1081-1083.

46. Ren Q, Barber HK, Crawford GL, et al. Endobrevin/VAMP-8 Is the primary v-SNARE for the platelet release reaction. *Mol Biol Cell.* 2007;18(1):24-33.

47. Kahr WHA. Granules and thrombus formation. *Blood.* 2009;114(5):932-933.

48. Puri N, Roche PA. Mast cells possess distinct secretory granule subsets whose exocytosis is regulated by different SNARE isoforms. *Proc Natl Acad Sci U S A.* 2008;105(7):2580-2585.

49. Feng D, Crane K, Rozenvayn N, Dvorak AM, Flaumenhaft R. Subcellular distribution of 3 functional platelet SNARE proteins: human cellubrevin, SNAP-23, and syntaxin 2. *Blood.* 2002;99(11):4006-4014.